PHYSICAL REVIEW B **90**, 121111(R) (2014)

Lifting of xz/yz orbital degeneracy at the structural transition in detwinned FeSe

T. Shimojima,[1,*] Y. Suzuki,[1] T. Sonobe,[1] A. Nakamura,[1] M. Sakano,[1] J. Omachi,[2] K. Yoshioka,[3] M. Kuwata-Gonokami,[2,3] K. Ono,[4] H. Kumigashira,[4] A. E. Böhmer,[5] F. Hardy,[5] T. Wolf,[5] C. Meingast,[5] H. v. Löhneysen,[5,6] H. Ikeda,[7] and K. Ishizaka[1]

[1]*Quantum-Phase Electronics Center (QPEC) and Department of Applied Physics, The University of Tokyo, Bunkyo, Tokyo 113-8656, Japan*

[2]*Photon Science Center, The University of Tokyo, 7-3-1 Hongo, Bunkyo-ku, Tokyo 113-8656, Japan*

[3]*Department of Physics, The University of Tokyo, 7-3-1 Hongo, Bunkyo-ku, Tokyo 113-0033, Japan*

[4]*KEK, Photon Factory, Tsukuba, Ibaraki 305-0801, Japan*

[5]*Institut für Festkörperphysik, Karlsruhe Institute of Technology, 76021 Karlsruhe, Germany*

[6]*Physikalisches Institut, Karlsruhe Institute of Technology, 76128 Karlsruhe, Germany*

[7]*Department of Physics, Kyoto University, Kyoto 606-8502, Japan*

(Received 4 July 2014; revised manuscript received 11 September 2014; published 29 September 2014)

We study superconducting FeSe ($T_c = 9$ K) exhibiting the tetragonal-orthorhombic structural transition ($T_s \sim 90$ K) without any antiferromagnetic ordering, by utilizing angle-resolved photoemission spectroscopy. In the detwinned orthorhombic state, the energy position of the d_{yz} orbital band at the Brillouin zone corner is 50 meV higher than that of d_{xz}, indicating the orbital order similar to the NaFeAs and $BaFe_2As_2$ families. Evidence of orbital order also appears in the hole bands at the Brillouin zone center. Precisely measured temperature dependence using strain-free samples shows that the onset of the orbital ordering (T_o) occurs very close to T_s, thus suggesting that the electronic nematicity above T_s is considerably weaker in FeSe compared to $BaFe_2As_2$ family.

DOI: 10.1103/PhysRevB.90.121111 PACS number(s): 79.60.−i, 74.70.Xa, 75.25.Dk

The parent compounds of iron-based superconductors [1] mostly exhibit complex phase transitions characterized by the antiferromagnetic (AFM) transition at T_N occurring simultaneously with or just below the tetragonal-orthorhombic structural transition at T_s [2]. These phase transitions are similarly suppressed toward the appearance of the superconducting phase by partial chemical substitution or applying pressure [3], indicating a strong relation between magnetism, superconductivity, and lattice deformation. Recently, systematic x-ray diffraction and torque magnetometry measurements on P-doped $BaFe_2As_2$ (Ba122) further revealed an in-plane anisotropy developing at T^* above T_s and T_N [4], i.e., an electronic nematicity. The nematic susceptibility in Co- and K-doped Ba122 extracted from the elastic shear modulus [5] and thermal expansion [6], on the other hand, do not show any anomalies suggestive of a fourfold symmetry reduction above T_s [5].

In association with the above-mentioned complex phase diagram, theoretical studies raised the possibility of orbital ordering (OO) [7–9] characterized by the nonequivalent electronic occupation in Fe $3d_{xz}$ (xz) and d_{yz} (yz) orbitals, which may couple the AFM and lattice deformation. Polarization-dependent laser angle-resolved photoemission spectroscopy (ARPES) indeed reported nearly orbital-polarized Fermi surfaces (FSs) in the AFM state of nondoped Ba122, suggestive of an orbital-ordered state [10]. Later, ARPES studies on lightly Co-doped [11] and P-doped Ba122 [12] reported the nonequivalent shifts of the xz/yz orbitals appearing above T_s, thus suggesting the possible interplay between the electronic nematicity and the orbital anisotropy. The theoretical origin of the electronic nematicity is based on either magnetism [13–17] or orbital degrees of freedom [7–9,18]. In the former, Z_2 spin-nematic ordering triggers the orthorhombic lattice distortion and xz/yz OO. On the other hand, the latter scenario defines the order parameter of the ferro-OO as $|N_{xz} - N_{yz}|$, where N_{xz} and N_{yz} represent the number of occupied xz and yz states below the Fermi level (E_F). $|N_{xz} - N_{yz}|$ naturally reduces the symmetry from fourfold to twofold, leading to the orthorhombic transition and the FS nesting-driven AFM state [18].

The electronic structures of the respective phases thus have been investigated both theoretically and experimentally. Nevertheless, it is difficult to separately distinguish and evaluate the effects of AFM and OO, since in most cases they are closely coupled in a narrow temperature (T) range. Recently, NaFeAs (Na111) possessing fairly well separated transition temperatures of $T_s = 53$ K and $T_N = 40$ K, has been investigated by ARPES [19,20]. In Na111, the OO was found to develop just at or slightly above T_s, which seems to trigger the stripe AFM order at lower T_N, due to the evolution of the twofold anisotropic FSs [19,20]. On the other hand, FeSe is a peculiar system among iron-based superconductors. It has the simplest crystal structure and undergoes a tetragonal-orthorhombic structural transition at around 90 K without any AFM ordering [21]. The absence of the AFM transition in FeSe poses some questions on the existence of the OO and its relation to the origin of the structural transition. Precise ARPES measurements on FeSe will offer valuable insight into the interplay between the electronic and the lattice degrees of freedom, which seems to strongly depend on the material class in the iron-based superconductors.

In this work, the electronic structure of FeSe is investigated by using lasers, a He-discharge lamp, and synchrotron-radiation ARPES. Nonequivalent energy shifts of xz/yz orbital bands are found to arise below T_s. The result from the detwinned sample clearly shows that the yz orbital is located at 50 meV higher energy compared to xz, at the Brillouin zone (BZ) corners. This large energy difference suggests an electronic origin of the nonequivalent xz/yz orbitals, namely, OO. The good correspondence between T_s and T_o indicates

*Corresponding author: shimojima@ap.t.u-tokyo.ac.jp

that the structural transition in FeSe is simultaneously driven by the OO.

Single crystals of FeSe were synthesized as described elsewhere [21]. The transition temperatures of the single crystals were estimated to be $T_s \sim 90$ K and $T_c = 9.8$ K from the resistivity. We used a variety of light sources and electron spectrometers. Overall ARPES measurements were performed using a VG-Scienta SES2002 analyzer and synchrotron radiation of 60 eV at BL28A of Photon Factory. Circular-polarized light was used with the total energy resolution of 20 meV. For the hole bands at BZ center, a combination of a VG-Scienta R4000WAL electron analyzer and the fourth-harmonic generation of Ti:sapphire laser radiation ($h\nu = 5.9$ eV) [22] was used at the University of Tokyo [23] to perform measurements of polarization dependence (s,p) and high energy resolution (3 meV). For the BZ corners of the detwinned single crystals, we used VG-Scienta R4000WAL analyzer and a helium discharge lamp of $h\nu = 21.2$ eV at the University of Tokyo, to fully utilize the six-axis goniometer that can rotate the azimuthal angle of the detwinned sample *in situ*. The energy resolution was set to 10 meV. To detwin the single crystals, we applied the tensile strain along one of the tetragonal (π,π) directions, which brings the orthorhombic a^o axis ($a^o > b^o$) along its direction below T_s. Samples were cleaved *in situ* at $T = 200$ K in an ultrahigh vacuum of 7×10^{-11} Torr. Band calculations were performed based on density functional theory (DFT) using the WIEN2K package [24]. Lattice parameters used for the calculations were taken from Ref. [25].

The band calculation of FeSe in the tetragonal phase shows quasi-two-dimensional FSs as depicted in Fig. 1(a). The mapping of ARPES intensity at $E_F \pm 5$ meV for strain-free FeSe [Fig. 1(b)], measured at 120 K and $h\nu = 60$ eV, shows FSs similar to the calculation; the hole and electron FSs are located at the tetragonal BZ center (Γ) and corners (M), respectively. Band dispersions in both tetragonal [120 K, Fig. 1(d)] and orthorhombic [20 K, Fig. 1(g)] phases were taken along the momentum cut indicated by the white arrow in Fig. 1(b). Note that since the crystal at $T < T_s$ is composed of twinned orthorhombic domains, the band dispersions along k_x and k_y become overlapped in the ARPES image as schematically shown in Fig. 1(c).

Figures 1(d) and 1(e) show the ARPES image at 120 K and corresponding band dispersion obtained by plotting the peaks of momentum distribution curves (MDCs, with horizontal error bars) and energy distribution curves (EDCs, with vertical error bars). One can identify two electron bands (δ_e,ε_e) and two hole bands (δ_h,ε_h) around the M point. According to the calculations, δ and ε bands are mainly composed of xy and xz/yz orbital characters, respectively. On cooling, the band dispersions exhibit drastic changes in both number and energy position as shown in Fig. 1(g). The most prominent features appearing at $T = 20$ K are the shallow electronlike band with its bottom just below E_F and the holelike band showing its maximum at $E - E_F = -50$ meV at the M point, where $E - E_F$ represents the energy relative to E_F. Some additional band dispersions are also recognized at $0.2 - 0.4$ Å^{-1} away from the M point. By plotting the peaks of EDCs and MDCs, and by assuming a symmetric dispersion with respect to the M point, we can identify three electron bands (δ_e,ε'_e,ε''_e) and three

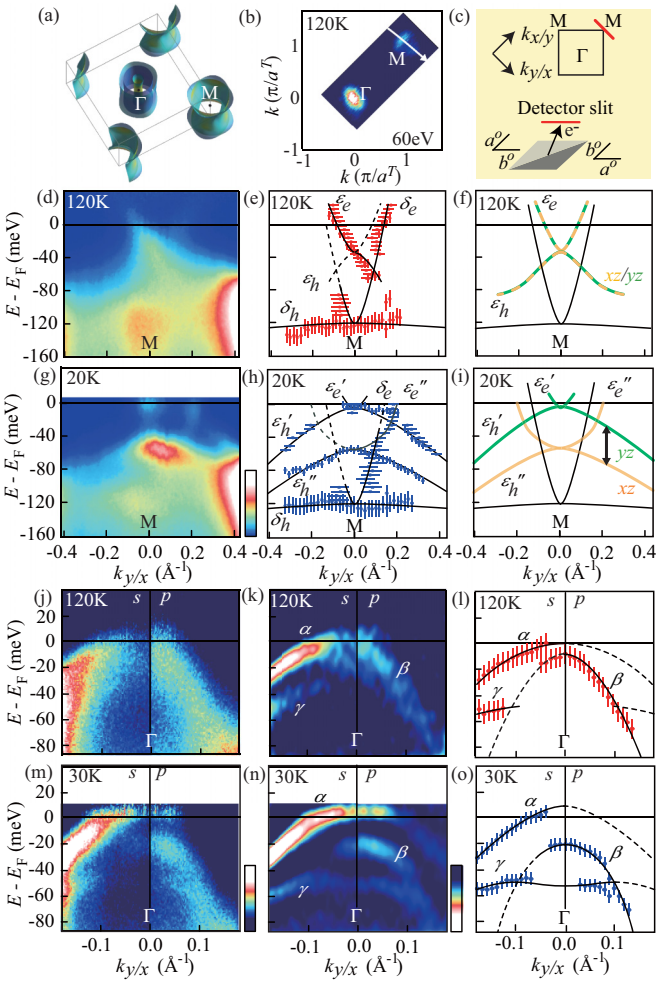

FIG. 1. (Color online) (a) Calculated FSs in the tetragonal phase of FeSe. (b) FSs in the tetragonal phase detected with the circular-polarized photons of $h\nu = 60$ eV. The white arrow indicates the momentum cut in (d)–(i). (c) Schematics of the twinned domains in the orthorhombic phase, where M along k_x and M along k_y are overlapped below T_s. (d) ARPES image ($h\nu = 60$ eV) at the BZ corner for 120 K ($T_s < T$) divided by the Fermi-Dirac (FD) function. (e) MDC and EDC peak plots with the band assignment, and (f) the schematically drawn band dispersions. Black curves in (e) indicate the band dispersions estimated from the peak positions. (g)–(i) Similar to (d)–(f) recorded at 20 K ($T < T_s$). The black arrow indicates the relative energy between the xz and yz orbitals. (j) ARPES image ($h\nu = 5.9$ eV) at the BZ center for 120 K ($T_s < T$) divided by FD function. (k) Its second E derivative and (l) the band dispersions with peak plots. Left (right) side in (j) and (k) show the ARPES data taken by s (p) polarization. (m)–(o) Similar to (j)–(l) recorded at 30 K ($T < T_s$).

hole bands (δ_h,ε'_h,ε''_h) at 20 K, as depicted in Fig. 1(h). Note that the δ_h and δ_e bands composed of xy orbitals are almost T independent.

The increase in the number of ε_e and ε_h bands is consistently explained by considering both the lifting of degeneracy in the xz/yz bands (i.e., OO) and the formation of the twinned domains below T_s. As already discussed [11,12], OO in twinned crystals doubles the number of observed xz/yz bands around the BZ corners, due to the overlap of nonequivalent k_x and k_y orientations. We can thus derive the xz/yz OO

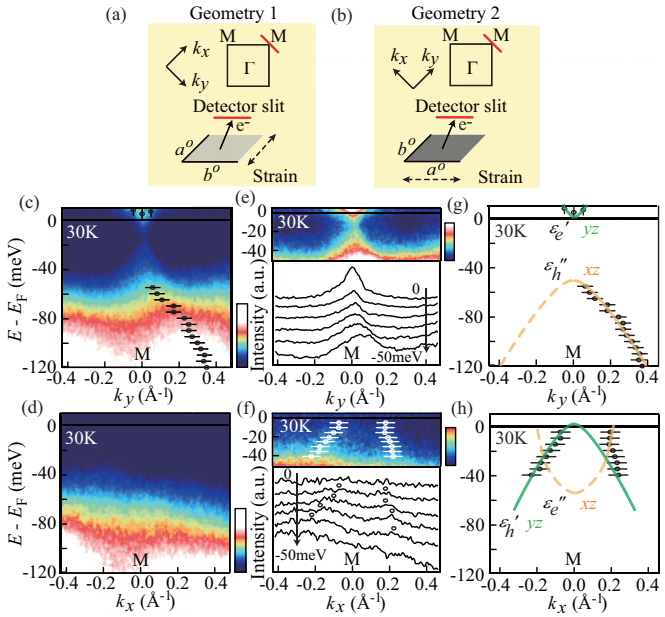

FIG. 2. (Color online) (a), (b) Two experimental geometries for ARPES ($h\nu = 21.2$ eV) on detwinned samples. The direction of the tensile strain is shown by the broken arrows, with respect to the detector slit. Band dispersions along k_y (k_x) are detected in geometry 1 (2). (c), (d) ARPES images divided by the FD function, taken along k_y and k_x, respectively. (e), (f) Upper panels show the high-contrast ARPES image near E_F along k_y and k_x, respectively. Lower panels show the MDCs from E_F to -50 meV. (g), (h) Peak plots and schematic band dispersions along k_y and k_x, respectively.

appearing as the splitting of ε hole and electron bands, as schematically shown in Fig. 1(i).

The impact of the OO also shows up at the BZ center. Around the Γ point in the tetragonal phase (120 K), as shown in Fig. 1(j), there are three hole bands (α,β,γ) observed with different gradients. The second E derivative of the ARPES image [Fig. 1(k)] emphasizes that α and γ bands (β band) are clearly detected by s (p) -polarization configuration. The band dispersions in Fig. 1(l) show that the α and β bands are nearly degenerate at the BZ center, whereas the γ band is located at around $E - E_F = -50$ meV. At 30 K, the multiple structure of the bands at the BZ center becomes clearer [Figs. 1(m) and 1(n)]. The energy positions of the α, β, and γ hole bands in the orthorhombic phase, as shown in Fig. 1(o), are consistent with previous ARPES on FeSe [26,27]. Reference [26] reported that α and β hole bands predominantly include xz/yz orbital character, which is consistent with the observed opposite polarization dependencies of α and β bands [Figs. 1(m) and 1(n)]. As schematically shown in Fig. 1(o), the separation between the α and β bands at the Γ point at 30 K is estimated to be $\sim$30 meV, considerably larger than at 120 K. This energy scale is nearly comparable to that found for the xz/yz OO at the BZ corners.

To conclusively assign the xz and yz orbital components at the BZ corners, we use the detwinned single crystals. As illustrated in Figs. 2(a) and 2(b), the k_y and k_x directions are separately recorded at the M point, by using geometries 1 and 2. The obtained ARPES images along k_y and k_x are shown in Figs. 2(c) and 2(d), respectively. In Fig. 2(c), the electronlike ε_e' band touching E_F and the holelike ε_h'' band at $E - E_F = -50$ meV can be identified, while they are absent in Fig. 2(d). In the enhanced color scale as shown in Figs. 2(e) and 2(f), on the other hand, a holelike ε_h' band approaching E_F becomes visible only in geometry 2. These observations of band dispersions at the M point along k_y and k_x are summarized in Figs. 2(g) and 2(h), by plotting the EDC and MDC peaks. According to the band calculations on FeSe, the yz (xz) orbital forms a saddle point at the BZ corner, with the electronlike band along the k_y (k_x) and the holelike band along the k_x (k_y) direction. The present ARPES data on detwinned single crystals indicates an upward (downward) shift of the yz (xz) orbital band on cooling. We mention that the direction of the energy shift in the xz/yz orbital bands of FeSe is also common to the Ba122 and Na111 systems.

Now we move on to the detailed T dependence of the band dispersions at the BZ corner across T_s. Here we used the strain-free twinned single crystals to extract the intrinsic T dependence, without the influence of uniaxial pressure. Figures 3(a)–3(f) show the second E derivative of the ARPES image at the M point. In the image at 50 K as shown in Fig. 3(a), the ε_e', ε_e'', and ε_h'' bands are clearly emphasized. By tracking the ε_e' and ε_h'' bands, respectively representing the yz and xz orbitals, a drastic change appears at 90 K [Fig. 3(d)]. Above 90 K, the xz/yz orbital bands become degenerate and almost T independent.

In order to precisely estimate the onset T of the xz/yz OO, the EDCs at the M point are shown for 20–140 K in

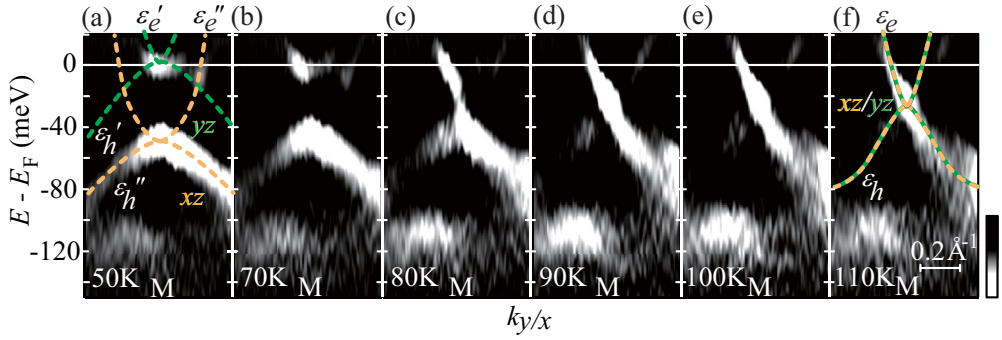

FIG. 3. (Color online) (a)–(f) T dependence of the second E derivative of ARPES images taken at 50, 70, 80, 90, 100, and 110 K at the twinned M point ($h\nu = 60$ eV).

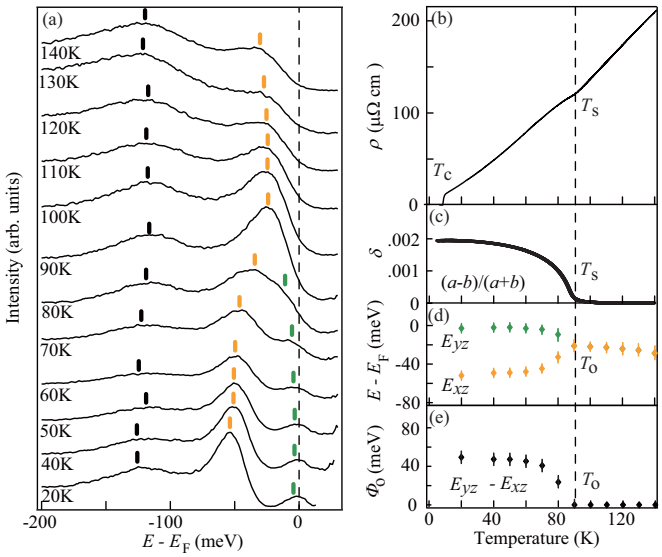

FIG. 4. (Color online) (a) T dependence of the EDCs at the M point divided by the FD functions. Peak energies of $\varepsilon'_e(yz)$, $\varepsilon''_h(xz)$, and $\delta_h(xy)$ bands are denoted by green, orange, and black markers. (b) T dependence of the in-plane resistivity ρ, (c) orthorhombicity $\delta(T) = (a-b)/(a+b)$ [21], (d) energy of the xz and yz orbital bands E_{xz} and E_{yz}, and (e) the OO parameter $\Phi_o(T) = E_{yz} - E_{xz}$.

Fig. 4(a). The peak positions of the EDCs can be determined by the bottom positions of the second-derivative curves (not shown). At 20 K, the peaks of the EDC are located at 3, 55, and 115 meV, corresponding to $\varepsilon'_e(yz)$, $\varepsilon''_h(xz)$, and $\delta_h(xy)$ bands, respectively. With increasing T, the two peaks of ε'_e and ε''_h get closer and merge into a single peak at ∼90 K, in contrast to the δ_h band (xy), which remains nearly T independent. The peak energies of EDC for the ε'_e and ε''_h bands, E_{yz} and E_{xz}, are plotted in Fig. 4(d). This clearly indicates that the energetically nonequivalent xz and yz orbitals become degenerate at 90 K.

The order parameter of the OO, as we here define by $\Phi(T) = E_{yz} - E_{xz}$, shows the value of $\Phi_o \sim 50$ meV at the lowest T, with $T_o \sim 90$ K [Fig. 4(e)]. $\Phi_o \sim 50$ meV is significantly larger than expected if driven only by the orthorhombic lattice distortion (estimated to be <10 meV by DFT calculation for FeSe). This indicates that the value $\Phi_o \sim 50$ meV is evidence of an electronically driven OO. On the other hand, T_s of the FeSe single crystal was estimated to be ∼90 K by electrical resistivity [Fig. 4(b)] and thermal expansion measurements [Fig. 4(c)] [21]. The close correspondence between T_o and T_s may suggest that the structural transition itself is triggered by OO. At the same time, it also indicates that the electronic nematicity above T_s is severely weaker in FeSe compared to the Ba122 family.

Here we find that the 122, 111, and 11 families show OO of similar behavior, i.e., $E_{yz} > E_{xz}$ at the BZ corners, on cooling. It is also worth mentioning that the OO always appears at the highest T of all phase transitions. These facts suggest that the OO may be a ubiquitous feature in iron-based superconductors that drives the twofold symmetric properties in the FeAs or FeSe layers. On the other hand, the relation among T_s, T_N, and T_o is considerably material dependent. How the OO triggers the structural and magnetic transitions, in some cases appearing as the electronic nematicity at higher T, seems to depend strongly on the specific material.

The present ARPES result, clearly showing the lifting of xz/yz orbital degeneracy, suggests that the shapes of the FSs at the BZ center and corners are modified to a twofold symmetry. Such a distortion of the FSs below an OO transition has also been discussed for Na111, as a possible origin of the stripe-type AFM ordering [19]. Theoretical studies including the momentum-independent nonequivalency of the xz/yz orbital reported the enhancement of the magnetic susceptibility along the (0,0)-(π,0) direction [18]. This scenario may explain the enhancement of the spin fluctuations in FeSe observed below ∼100 K in the orbitally ordered state [28]. The interorbital fluctuations can also simultaneously arise from FS nesting between different orbital bands due to the vertex corrections [29]. These spin and/or orbital fluctuations may be playing important roles for superconductivity. Considering its fairly ubiquitous occurrence across the families, this OO can be regarded as one of the prerequisites for superconductivity in iron-based superconductors.

In conclusion, we investigated the precise electronic structure of superconducting FeSe, across the structural phase transition. By using detwinned single crystals, the saddle point of the band at the BZ corners consisting of the yz orbital was found to be located at 50 meV higher than that of xz, indicating OO. The effect of xz/yz OO also appeared in the hole bands at the BZ center. From the detailed T dependence, the OO was found to show up at T very close to T_s, thus implying the orbital origin of the orthorhombic transition in FeSe. By comparing with other families (Ba122 and Na111), the ubiquitous nature of OO in iron-based superconductors is suggested, whereas the electronic nematicity above T_s might be considerably weaker for FeSe.

We acknowledge Y. Matsuda, T. Shibauchi, S. Kasahara, H. Kontani, S. Onari, K. Okazaki, and S. Shin for valuable discussions. Synchrotron-radiation ARPES experiments were carried out at BL-28A at Photon Factory (Proposal No. 2012G751). This research was supported by Toray Science Foundation; Precursory Research for Embryonic Science and Technology (PRESTO), Japan Science and Technology Agency; the Photon Frontier Network Program of the MEXT, Japan; and Research Hub for Advanced Nano Characterization, The University of Tokyo, supported by MEXT, Japan.

[1] Y. Kamihara, T. Watanabe, M. Hirano, and H. Hosono, J. Am. Chem. Soc. **130**, 3296 (2008).

[2] M. Rotter, M. Tegel, D. Johrendt, I. Schellenberg, W. Hermes, and R. Pöttgen, Phys. Rev. B **78**, 020503 (2008).

[3] S. Kasahara, T. Shibauchi, K. Hashimoto, K. Ikada, S. Tonegawa, R. Okazaki, H. Shishido, H. Ikeda, H. Takeya, K. Hirata, T. Terashima, and Y. Matsuda, Phys. Rev. B **81**, 184519 (2010).

[4] S. Kasahara, H. J. Shi, K. Hashimoto, S. Tonegawa, Y. Mizukami, T. Shibauchi, K. Sugimoto, T. Fukuda, T. Terashima, Andriy H. Nevidomskyy, and Y. Matsuda, Nature (London) **486**, 382 (2012).

[5] A. E. Böhmer, P. Burger, F. Hardy, T. Wolf, P. Schweiss, R. Fromknecht, M. Reinecker, W. Schranz, and C. Meingast, Phys. Rev. Lett. **112**, 047001 (2014).

[6] C. Meingast, F. Hardy, R. Heid, P. Adelmann, A. E. Böhmer, P. Burger, D. Ernst, R. Fromknecht, P. Schweiss, and T. Wolf, Phys. Rev. Lett. **108**, 177004 (2012).

[7] F. Kruger, S. Kumar, J. Zaanen, and J. V. Brink, Phys. Rev. B **79**, 054504 (2009).

[8] W. Lv, J. Wu, and P. Phillips, Phys. Rev. B **80**, 224506 (2009).

[9] C. Lee, W.-G. Yin, and W. Ku, Phys. Rev. Lett. **103**, 267001 (2009).

[10] T. Shimojima, K. Ishizaka, Y. Ishida, N. Katayama, K. Ohgushi, T. Kiss, M. Okawa, T. Togashi, X.-Y. Wang, C.-T. Chen, S. Watanabe, R. Kadota, T. Oguchi, A. Chainani, and S. Shin, Phys. Rev. Lett. **104**, 057002 (2010).

[11] M. Yi, D. Lu, J.-H. Chu, J. G. Analytis, A. P. Sorini, A. F. Kemper, B. Moritz, S.-K. Mo, R. G. Moore, M. Hashimoto, W.-S. Lee, Z. Hussain, T. P. Devereaux, I. R. Fisher, and Z.-X. Shen, Proc. Natl. Acad. Sci. **108**, 6878 (2011).

[12] T. Shimojima, T. Sonobe, W. Malaeb, K. Shinada, A. Chainani, S. Shin, T. Yoshida, S. Ideta, A. Fujimori, H. Kumigashira, K Ono, Y. Nakashima, H. Anzai, M. Arita, A. Ino, H. Namatame, M. Taniguchi, M. Nakajima, S. Uchida, Y. Tomioka, T. Ito, K. Kihou, C. H. Lee, A. Iyo, H. Eisaki, K. Ohgushi, S. Kasahara, T. Terashima, H. Ikeda, T. Shibauchi, Y. Matsuda, and K. Ishizaka, Phys. Rev. B **89**, 045101 (2014).

[13] C. Fang, H. Yao, W.-F. Tsai, J. Hu, and S. A. Kivelson, Phys. Rev. B **77**, 224509 (2008).

[14] C. Xu, M. Muller, and S. Sachdev, Phys. Rev. B **78**, 020501(R) (2008).

[15] R. M. Fernandes, L. H. VanBebber, S. Bhattacharya, P. Chandra, V. Keppens, D. Mandrus, M. A. McGuire, B. C. Sales, A. S. Sefat, and J. Schmalian, Phys. Rev. Lett. **105**, 157003 (2010).

[16] R. M. Fernandes, A. V. Chubukov, J. Knolle, I. Eremin, and J. Schmalian, Phys. Rev. B **85**, 024534 (2012).

[17] R. M. Fernandes, A. V. Chubukov, and J. Schmalian, Nat. Phys. **10**, 97 (2014).

[18] H. Kontani, T. Saito, and S. Onari, Phys. Rev. B **84**, 024528 (2011).

[19] M. Yi, D. H. Lu, R. G. Moore, K. Kihou, C.-H. Lee, A. Iyo, H. Eisaki, T. Yoshida, A. Fujimori, and Z.-X. Shen, New J. Phys. **14**, 073019 (2012).

[20] Y. Zhang, C. He, Z. R. Ye, J. Jiang, F. Chen, M. Xu, Q. Q. Ge, B. P. Xie, J. Wei, M. Aeschlimann, X. Y. Cui, M. Shi, J. P. Hu, and D. L. Feng, Phys. Rev. B **85**, 085121 (2012).

[21] A. E. Böhmer, F. Hardy, F. Eilers, D. Ernst, P. Adelmann, P. Schweiss, T. Wolf, and C. Meingast, Phys. Rev. B **87**, 180505(R) (2013).

[22] J. Omachi, K. Yoshioka, and M. Kuwata-Gonokami, Opt. Express **20**, 23542 (2012).

[23] There is some uncertainty in the in-plane momentum obtained by low-energy ARPES, due to the effect of work function. On transforming emission angle to the momentum, we referred to the data recorded using $h\nu = 40.8\,\mathrm{eV}$, where the α hole band exhibited nearly comparable Fermi momentum and band gradient to $h\nu = 5.9\,\mathrm{eV}$.

[24] P. Blaha, K. Schwarz, G. K. H. Madsen, D. Kvasnicka, and J. Luitz, *WIEN2K, An Augmented Plane Wave Plus Local Orbitals Program for Calculating Crystal Properties* (Karlheinz Schwarz, Techn. Universitat Wien, Austria, 2001).

[25] S. Margadonna, Y. Takabayashi, M. T. McDonald, K. Kasperkiewicz, Y. Mizuguchi, Y. Takano, A. N. Fitch, E. Suarde, and K. Prassides, Chem. Commun. **43**, 5607 (2008).

[26] J. Maletz, V. B. Zabolotnyy, D. V. Evtushinsky, S. Thirupathaiah, A. U. B. Wolter, L. Harnagea, A. N. Yaresko, A. N. Vasiliev, D. A. Chareev, A. E. Böhmer, F. Hardy, T. Wolf, C. Meingast, E. D. L. Rienks, B. Buchner, and S. V. Borisenko, Phys. Rev. B **89**, 220506(R) (2014).

[27] K. Nakayama, Y. Miyata, G. N. Phan, T. Sato, Y. Tanabe, T. Urata, K. Tanigaki, and T. Takahashi, arXiv:1404.0857.

[28] T. Imai, K. Ahilan, F. L. Ning, T. M. McQueen, and R. J. Cava, Phys. Rev. Lett. **102**, 177005 (2009).

[29] S. Onari and H. Kontani, Phys. Rev. Lett. **109**, 137001 (2012).